Improved carrier transport in Mn:ZnSe quantum dots sensitized La-doped nano-TiO_2 thin film*

Shao Li(李绍), Gang Li(李刚), Li-Shuang Yang(杨丽爽), and Kui-Ying Li(李葵英)†

State Key Laboratory of Metastable Materials Science and Technology, College of Materials Science and Engineering, Yanshan University, Qinhuangdao 066004, China

(Received 16 December 2019; revised manuscript received 28 January 2020; accepted manuscript online 18 February 2020)

Mn:ZnSe/ZnS/L-Cys core-shell quantum dots (QDs) sensitized La-doped nano-TiO_2 thin film (QDSTF) was prepared. X-ray photoelectron spectroscopy (XPS), nanosecond transient photovoltaic (TPV), and steady state surface photovoltaic (SPV) technologies were used for probing the photoelectron behaviors in the Mn-doped QDSTF. The results revealed that the Mn-doped QDSTF had a p-type TPV characteristic. The bottom of the conduction band of the QDs as a sensitizer was just 0.86 eV above that of the La-doped nano-TiO_2 thin film, while the acceptor level of the doped Mn^{2+} ions was located at about 0.39 eV below and near the bottom of the conduction band of the QDs. The intensity of the SPV response of the Mn-doped QDSTF at a specific wavelength was ∼2.1 times higher than that of the undoped QDSTF. The region of the SPV response of the Mn-doped QDSTF was extended by 191 nm to almost the whole visible region as compared with the undoped QDSTF one. And the region of the TPV response of the Mn-doped QDSTF was also obviously wider than that of the undoped QDSTF. These PV characteristics of the Mn-doped QDSTF may be due to the prolonged lifetime and extended diffusion length of photogenerated free charge carriers injected into the sensitized La-doped nano-TiO_2 thin film.

Keywords: doping effects, ZnSe quantum dots sensitization, nano-TiO_2 thin film, photoelectron spectroscopy

PACS: 61.72.uj, 73.63.Kv, 82.80.Pv, 74.78.–w **DOI:** 10.1088/1674-1056/ab7742

1. Introduction

Quantum dots (QDs) have been widely studied over two decades[1–9] because of their unique electron structure characteristics such as tunability of the band gap,[10,11] size-dependent extinction coefficient,[12] and multiple exciton effect.[13] As a new material, various QDs are now being used in the fields of fluorescence labeling,[14] photonic crystals,[15,16] photoelectron and microelectron devices,[17] and the third generation solar cells.[18] At present, QDs sensitized solar cells (QDSSCs) have displayed potential applications especially in the renewable energy fields, and a big room for improvement in the photovoltaic (PV) conversion efficiency. Up to now, the study of II/VI group QDSSCs mainly focuses on broadening the visible light absorption range, and increasing the practical conversion efficiency close to the limit conversion efficiency of solar cells sensitized by the QDs.[19–27]

In our previous works, the self-assembled core-shell CdTe/CdS/ligand, CdSe/CdS/ligand, and ZnSe/ZnS/ligand QDs were prepared via the aqueous synthesis way, respectively.[28–31] The results revealed that the ligand and the shell layer played not negligible roles in the gradual energy band structure of these QDs. For examples, the ligand not only improved the stability of the QDs, but also may change the transport mechanism and adjust the transmission channel of photogenerated free charge carriers (FCCs) in these QDs. The outer-layer-ligand of these QDs as sensitizer played a molecular linker role between the QDs and nano-TiO_2 substrate, except for those functions mentioned above. The shell layer such as CdS or ZnS in these QDs should be responsible for the obvious quantum confinement effect in these quantum systems, mainly because the energy band of the shell layer was located in between those of the core and the outer layer ligand. The study confirmed that ZnSe QDs-sensitized nano-TiO_2 thin film (QDSTF) may become a potential candidate of photoanode, and the photoanodic properties probably determined the overall performance of QDSSCs, because the ZnSe QDs sensitizer has better surface photovoltaic (SPV) characteristics and lower toxicity than other members of II/VI semiconductors.[32] Moreover, some characteristic of the photoanode was closely related to the extended diffusion length of photogenerated FCCs and increased level of electron injection into the nano-TiO_2 substrate from the QDs sensitizer.[33]

It was reported that doped QDs can improve some performances of QDSSC.[34] In order to explore the effect of doping manganese in ZnSe QDs on the photoelectron characteristics of the QDSTF, in the present paper, Mn-doped ZnSe QDs were synthesized by a low temperature aqueous-phase method, and then Mn:ZnSe QDSTF was prepared by a modified chemical bath deposition (CBD) method. The assisting role of the La-doped mesoporous nano-TiO_2 substrate, for improving the carrier transport environment of the Mn:ZnSe QDSTF, was discussed in the paper. A series of photophysical phenomena of the Mn-doped QDSTF were probed via nanosecond

*Project supported by the Natural Science Foundation of Hebei Province, China (Grant No. E2017203029).

†Corresponding author. E-mail: kuiyingli@ysu.edu.cn

transient photovoltaic (TPV) and steady state SPV technologies, x-ray photoelectron spectroscopy (XPS), and UV-VIS absorption spectrum, supplemented by Fourier transform infrared (FTIR) spectrum, scanning electron microscopy (SEM), and laser Raman spectrum.

2. Experimental details

2.1. La-doped mesoporous nano-TiO_2 thin film preparation

First, La-doped mesoporous nano-TiO_2 powder was synthesized by the sol–gel method, in which polyethylene glycol was used as a template.[35,36] Figure S1 shows the adsorption–desorption curves and the distribution of the pore diameter of the as-prepared La-doped and undoped mesoporous TiO_2 nanocrystals. And the relevant surface parameters are listed in Table S1. Then, the La-doped nano-TiO_2 thin film was prepared by a knife coating method.[37] Briefly, the La-doped nano-TiO_2 slurry was formed by adding both the as-prepared La-doped TiO_2 nanoparticles and an appropriate quantity of α-turpentine into an ethyl cellulose ethanol solution. The slurry was stirred in the air until achieving an appropriate viscosity. Fluorine-doped tin oxide (FTO) glass was coated with the prepared TiO_2 slurry by the knife coating method. The coated FTO glass was calcined at 450 ℃ for 0.5 h. The first layer of the mesoporous La-doped nano-TiO_2 thin film was obtained. Multilayer films were obtained layer by layer in the same way. Figure S2 displays the x-ray diffraction (XRD) pattern of the prepared La-doped nano-TiO_2 powders and the La-doped nano-TiO_2 thin film with the thickness of approximately 21 μm, which was determined using a step measuring instrument.

2.2. Mn-doped ZnSe QDs synthesis and the QDSTF preparation

The modified aqueous synthesis of Mn-doped ZnSe QDs capped by L-Cys, similar to Ref. [29], involved the reaction between selenium-, zinc-, and manganese-precursors. First, the selenium precursor was prepared by mixing selenium powder with a $NaBH_4$ solution under stirring until the reaction was completed. The achieved selenium precursor with the concentration of sodium hydrogen selenide (NaHSe) equal to 0.167 mol/L was saved under the protection of nitrogen. Then, $Zn(CH_3COO)_2$, L-Cys, and $Mn(CH_3COO)_2$ were dissolved into deionized water with stirring and degassing with N_2 at pH 11 for 30 min. And then, the as-prepared Se-precursor was added to the above mixed solution. The Mn-doped ZnSe QDs solution was obtained after the mixed solution of selenium-, zinc- and manganese-precursors reacted at the room temperature in the atmosphere of nitrogen for 3 h.

Mn-doped ZnSe QDs sensitized La-doped nano-TiO_2 thin film was prepared by the CBD method.[38] Briefly, the TiO_2 thin film was placed at a certain angle in a beaker containing the Mn-doped ZnSe QDs solution, and then transferred with the beaker to an oil bath, deposited at 60 ℃ for 5 h. The sensitized thin film was taken out and rinsed with deionized water several times. Finally, the QDs sensitized thin film was obtained after it was dried at 60 ℃ for 0.5 h.

2.3. Characterizations

XRD (Rigaku D/max-2500/PC, Japan) was used to study the crystal structure of the as-prepared samples. The Brunauer–Emmett–Teller (BET) method (ASAP2020 HD88, USA) was used for detecting the specific surface area and porous structure of the as-prepared samples. XPS (Thermo ESCALAB 250 spectrometer with Al $K\alpha$ excitation 1486 eV, USA) was used to provide the information about the composition and valence state of the elements in the as-prepared QDs. SEM (Hitachi S-4800, Japan) was used to study the micromorphology of the as-prepared samples. Raman spectroscopy (Renishaw, England) was employed to inspect the molecular structure in the as-prepared nano-TiO_2 thin films.

In our experiment, SPV and TPV spectra of the as-prepared samples were detected by self-assembling devices, respectively. Details for the SPV and TPV measurements were described elsewhere.[39,40] SPV and TPV techniques can be used to obtain information on photoelectron behaviors at surfaces and phase interfaces because these techniques are by no means only sensitive to surfaces. Instead, they are sensitive to the entire surface space charge regions (SCRs) by super- or sub-band gap absorption, and even to buried interfaces located anywhere in the detected sample, as long as they can be reached by photons.[41]

3. Results and discussion

3.1. XPS analysis of Mn-doped ZnSe QDs

Figure 1 shows XPS of the as-prepared Mn-doped ZnSe QDs. The full XPS spectrum is displayed in Fig. 1(a). The characteristic peaks of C, Zn, Se, S, and Mn elements are displayed in Figs. 1(b)–1(f), respectively. Specifically, the two peaks that were loacted at 284.6 eV and 288.13 eV in Fig. 1(b) were related to the C–C and C=O bonds, respectively.[42–44] The binding energy of Zn $2p_{3/2}$ appeared at 1021.9 eV in Fig. 1(c), which was 0.5 eV higher than its standard peak position (1021.4 eV). This implied that the binding energy of the inner electron in Zn element of the QDs was increased. Therefore, the QDs were formed by core-ZnSe, shell-ZnS, and outlayer-ligand according to the results in Figs. 1(c)–1(e) and Refs. [45,46]. More importantly, the characteristic peak of Mn $2p_{3/2}$ was located at 641.8 eV in Fig. 1(f), which was in a good agreement with that of MnSe molecule.[47] This means that the Mn element was doped in Mn^{2+} ion form, which partly replaced the vacancy of Zn^{2+} ion and formed MnSe with Se^{2+}

ion. The XPS results of the Mn-doped ZnSe QDs were consistent with that of the XRD pattern of the sample in Fig. S3. According to Refs. [48,49], the valence band maximum (VBM) of a sample can be determined by the abscissa for the largest external tangent of the band of the VB spectrum. Therefore, the VBM of the as-prepared Mn:ZnSe/ZnS/L-Cys QDs was 1.34 eV as seen in Fig. 1(g), i.e., the energy level of the top of the valence band of the as-prepared QDs was 1.34 V (vs. H/H_2).

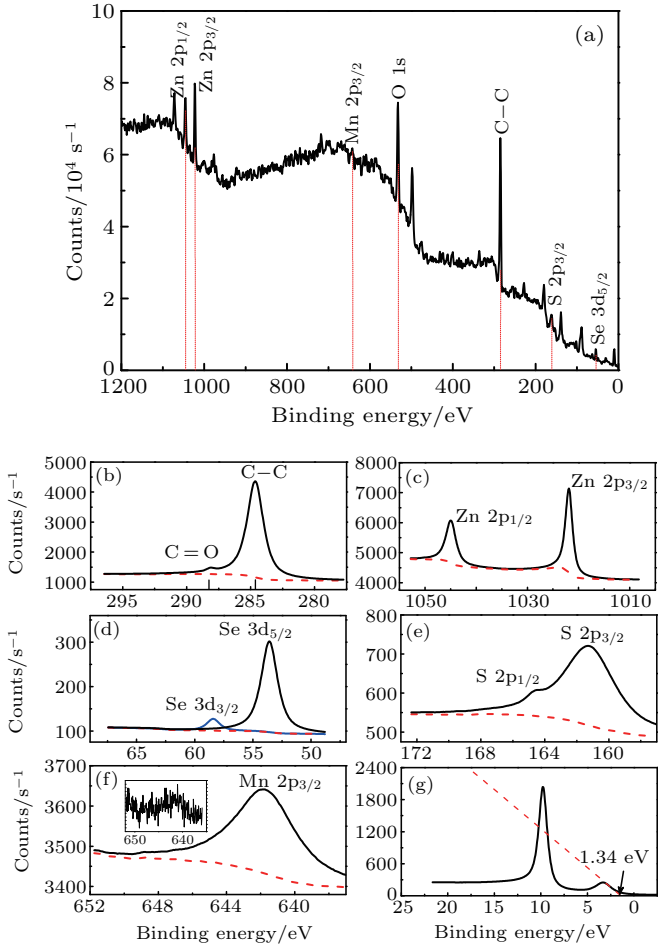

Fig. 1. XPS of as-prepared Mn-doped ZnSe/ZnS/L-Cys QDs. (a) Full spectrum; (b)–(f) qualitative elementary analysis of the QDs; (g) valence band spectrum of the QDs. Binding energy calibration is based on C 1s at 284.6 eV.

3.2. Microstructure of the QDs-sensitized nano-TiO_2 thin film

Figure 2 shows the SEM image of the mesoporous La-doped nano-TiO_2 thin film before and after sensitized by the Mn:ZnSe/ZnS/L-Cys QDs. The La-doped nano-TiO_2 substrate with the three-layer structure of approximately 21 μm was chosen according to our previous work.[50] The aggregation of the La-doped nano-TiO_2 particles at the substrate surface displayed the average size of 0.5 μm as shown in Fig. 2(a). The substrate thin film provided a good adsorption environment to the Mn-doped QDs sensitizer as shown in Fig. S1 and Table S1. The effect of La on the crystallization of nano-TiO_2 was measured in our previous work.[51] From Ref. [51], it can be inferred that the La-doping not only affects the surface photovoltaic character of nano-TiO_2, but also may improve the photogenerated carriers' transport in the prepared QDSTF. The micromorphology of the thin film sensitized by the Mn-doped QDs was superior to the substrate thin film in terms of the smoothness and the filling degree in Fig. 2(b).

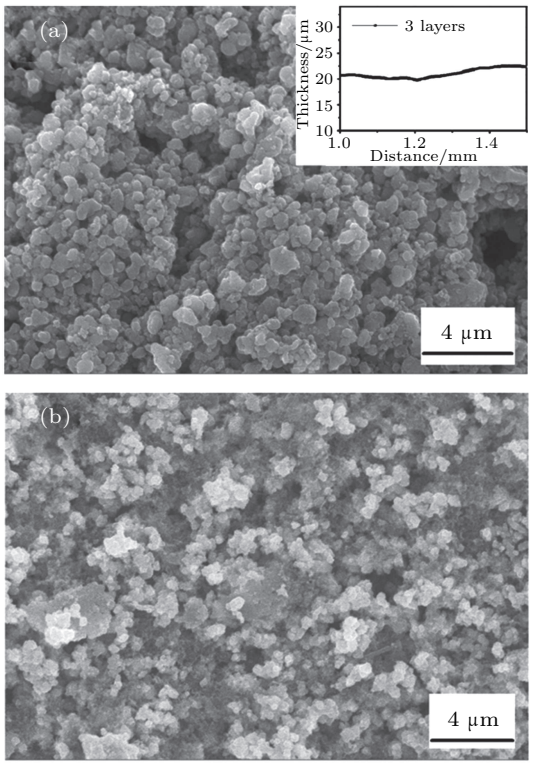

Fig. 2. SEM images of the mesoporous La-doped nano-TiO_2 thin film before sensitized (a) and after sensitized (b) by the Mn-doped ZnSe QDs. The inset in (a) gives the thickness of the nano-TiO_2 thin film with 3 layers. Film thicknesses were recorded by XP-2 Stylus Profilometer (USA).

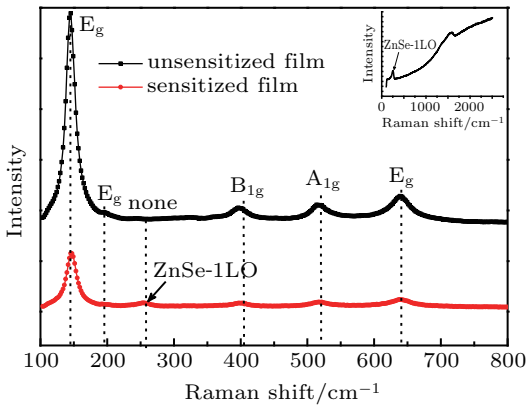

Fig. 3. Raman spectra of the nano-TiO_2 thin film before and after sensitized by the Mn-doped ZnSe QDs. Inset is the Raman spectrum of crystalline ZnSe. Laser: 532 nm edge (mode: regular).

Laser Raman spectra of the thin films before and after sensitized by the Mn-doped QDs are shown in Fig. 3. According to Ref. [52], anatase TiO_2 has six Raman vibration modes ($A_{1g} + 2B_{1g} + 3E_g$). Five of them appeared in the Raman spectrum of the substrate La-doped nano-TiO_2 thin film

in Fig. 3. This implied that the crystalline phase of the substrate thin film was mainly composed of anatase TiO_2. The anatase structure has better photoelectric property than the rutile phase.[53,54] It is noted that a Raman shift of the QDs sensitized thin film appeared at 253 cm^{-1} in Fig. 3. But, the Raman spectrum of the unsensitized thin film did not show the Raman shift at 253 cm^{-1} in Fig. 3. According to Ref. [55], the Raman shift was attributed to the longitudinal optical (1LO) vibration mode of ZnSe as seen in the inset of Fig. 3. The result confirmed that the Mn-doped ZnSe QDs had been adsorbed on the substrate thin film.

FTIR spectra of the as-prepared La-doped nano-TiO_2 thin film, undoped QDSTF, Mn-doped QDSTF, and pure L-Cys ligand are shown in Fig. 4. The peak located at 1634 cm^{-1} was identified to the stretching vibration of H–O–H bond of the adsorbed water molecules.[56] The peak at 1065 cm^{-1} was due to the stretching vibration of H–O–H bond.[57] As compared to the undoped QDSTF, the peak of the Mn-doped QDSTF disappeared at 1065 cm^{-1}, which implied that the doped Mn may inhibit the stretching vibration of H–O–H bond in the L-Cys ligand. The narrow peak at 2552 cm^{-1} resulted from the stretching vibration of –SH groups, which appeared in the FTIR spectrum of the pure L-Cys ligand, but disappeared in that of the two prepared QDs-sensitized thin films. The result suggested that the S–H bonds were broken during the formation of the two samples, and a ZnS shell layer was produced between the core-ZnSe and the outlayer ligand. This was in agreement with the results of XPS of the QDs in Fig. 1. In addition, the XRD pattern of the QDs in Fig. S3 confirmed the presence of the quasicrystal phase of ZnS in the QDs. Besides, the stretching vibration of –COOH at 1600 cm^{-1} disappeared in the spectra of the two QDSTFs. This was probably because the –COOH groups in the outlayer ligand of the QDs formed O–Ti–O chemical bonds with the dangling bonds on the surface of the nano-TiO_2 thin film. Therefore, the L-Cys ligand not only was a stabilizer of the QDs, but played a role of molecular linker between the QDs and the nano-TiO_2 thin film. For clarity, the wavenumbers corresponding to the main chemical bond vibrations of the four samples in Fig. 4 are listed in Table 1.

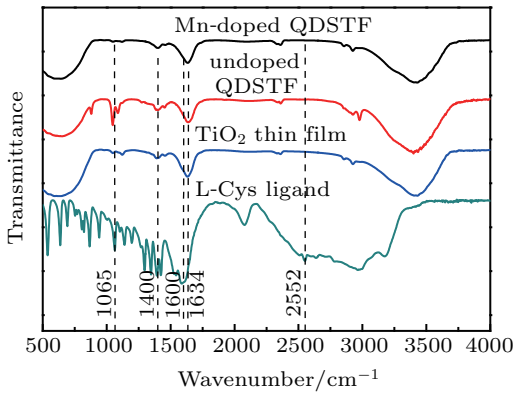

Fig. 4. FTIR spectra of the pure ligand L-Cys, the La-doped nano-TiO_2 thin film, the undoped QDSTF, and the Mn-doped QDSTF.

Table 1. Wavenumbers (cm^{-1}) corresponding to some chemical bond vibrations extracted from the FTIR spectra of the four samples.

Vibration mode	L-Cys ligand	Mn-doped QDSTF	Undoped QDSTF	TiO_2 thin film
υ_{S-H}	2552	–	–	–
υ^{awm}_{H-O-H}	1634	1634	1634	1634
υ^{as}_{COO}	1600	–	–	–
δ_{CH2}	1400	–	–	–
υ^{L-Cys}_{H-O-H}	1065	–	1065	–

υ: stretching vibration; δ: bending vibration; superscript as denotes asymmetry; superscript awm denotes adsorbed water molecules.

3.3. Photoelectron characteristics analysis

Room temperature UV-VIS absorption spectra of three types of nano-TiO_2 thin films are shown in Figs. 5(a)–5(c). An obvious redshift of the absorption band edges was displayed, from the absorption peak of the La-doped nano-TiO_2 thin film at 366 nm in Fig. 5(a) to that of the QDs-sensitized nano-TiO_2 thin film at 414 nm in Fig. 5(b), and to that of the Mn-doped QDs-sensitized nano-TiO_2 thin film at 450 nm (c_1) in Fig. 5(c). The optical band gaps, $E_{g,UV-VIS}$, were estimated by using the Tauc relation,[58] as seen in the insets of Figs. 5(a)–5(c) and listed in Table 2. The optical band gaps of the three thin films were 2.84 eV, 2.33 eV, and 1.71 eV, respectively, as shown in the insets of Fig. 5. That is, their band-to-band absorption edges were respectively 437 nm, 532 nm, and 725 nm, resulting in the absorption range of visible light gradually extended following the above sequence. The shoulder peak at 502 nm (c_2) in Fig. 5(c) may be closely related to the dopant Mn. Obviously, the wide absorption range for sunlight should be advantageous to the Mn-doped QDSTF as a photoanode.

Figure 6 shows the TPV spectroscopy of the as-prepared samples. It is interesting that the polarity of the TPV response of the undoped ZnSe QDs and the undoped QDSTF was positive, i.e., a positive TPV response, as shown in curves a_1 and b_1 in Figs. 6(a) and 6(b). Conversely, the negative polarity of the TPV response of the Mn-doped ZnSe QDs and Mn-doped QDSTF was shown in curves a_2 and b_2 in Figs. 6(a) and 6(b). According to the literature,[59] these Mn-doped samples had a p-type TPV characteristic because of their negative TPV response upon illuminating. The p-type TPV character-

istic resulted from the movement of negative charges, which arised from the electron–hole pairs caused by the illumination of laser pulse, from bulk to surface of the nanoparticles on the illuminated side. However, it was the opposite situation for these undoped samples. Therefore, it can be suggested that Mn dopant in the QDs probably contributed to change the direction of the photogenerated FCCs transport in the QDs and the QDs-sensitized thin film, on the basis of the change of the polarity of the TPV response of the sample before and after doping Mn element in Fig. 6.

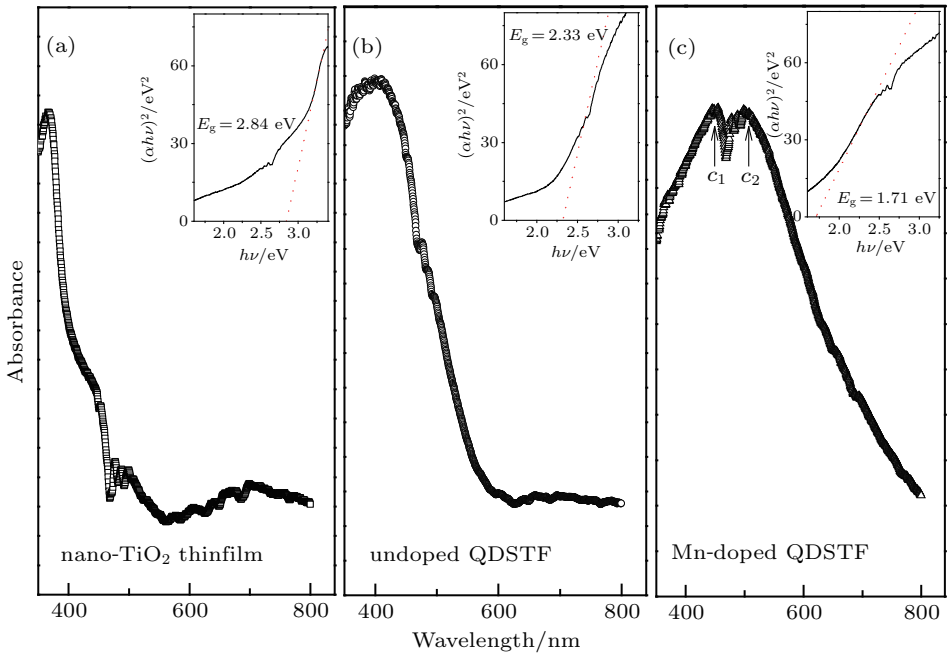

Fig. 5. Room-temperature UV-VIS absorption spectra of (a) the as-prepared La-doped nano-TiO_2 thin film, (b) undoped QDSTF, and (c) Mn-doped QDSTF. The corresponding Tauc relations are illustrated in the insets.

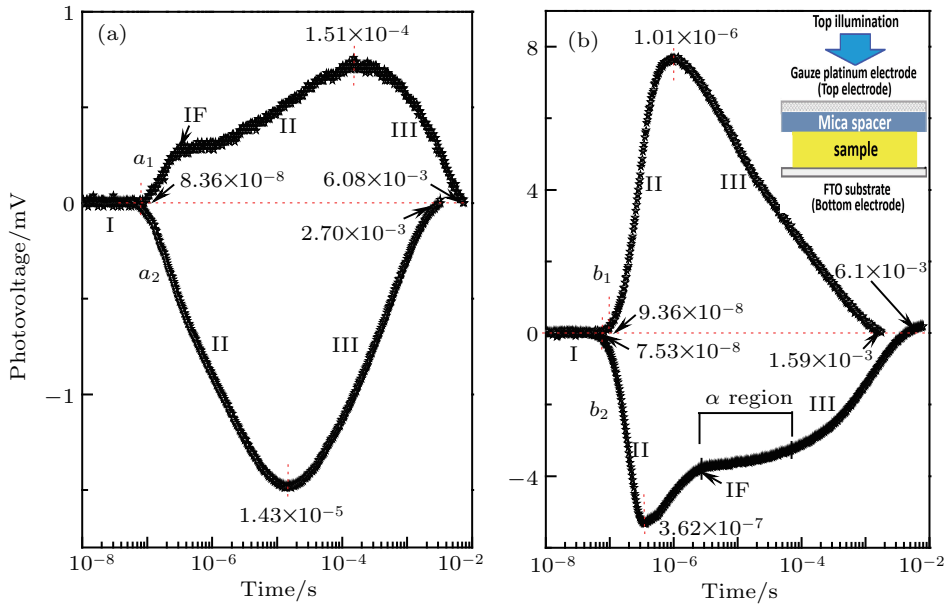

Fig. 6. TPV spectroscopy of (a) the undoped ZnSe QDs (a_1), the Mn-doped ZnSe QDs (a_2); (b) the undoped QDSTF (b_1), and the Mn-doped QDSTF (b_2). Inset in (b) illustrates the home-build setup for TPV spectrum measurement, where the sample was illuminated by a laser with a wavelength of 355 nm and an intensity of 20 μJ.

According to Ref. [60], the time range of the TPV response depends on the proportion of the thickness of SCR to the length of the photogenerated FCCs drift in SCR, and/or on the diffusion distance of the electron–hole pairs. Therefore, the diffusion length of the photogenerated electron-hole pairs in the Mn-doped QDSTF should be much larger than that in the undoped QDSTF, because the start time of the TPV response was ahead from 8.36×10^{-8} s to 7.53×10^{-8} s, and the end time was prolonged from 2.70×10^{-3} s to 6.10×10^{-3} s as compared the former to the latter, as shown in Fig. 6. In

a normal situation, the separation rate of electron–hole pairs is faster than their recombination rate before achieving the extrema of TPV responses. By contrast, the recombination rate is faster than the separation rate after the extrema is achieved according to Ref. [60]. Therefore, the range of the TPV response of each sample in Fig. 6 can be divided into three regions I, II, and III. Take the Mn-doped QDSTF as an example, the TPV response disappeared in region I of curve b_2 in Fig. 6(b) because photogenerated FCCs would not be produced until the time illuminated by the laser pulse reached 7.53×10^{-8} s. The absolute intensity of the negative TPV response in region II of curve b_2 in Fig. 6(b) increased before the illumination time reached 3.62×10^{-7} s, where the intensity of the negative TPV response was up to the maximum of 5.42 mV. In addition, an inflection point (IF) appeared at 2.8×10^{-6} s in region III of curve b_2 in Fig. 6(b). This may be due to the change in the proportion of the thickness of SCR to the diffusion length of electron–hole pairs in the process of photogenerated FCCs transport.[61] We propose that the inflection point may be closely related to a boundary that was crossed during charge migration from one SCR to another. In other words, the slope of the band in region III of curve b_2 in Fig. 6(b) may be changed when those photogenerated FCCs with negative charge moved from one SCR to another. Clearly, the recombination rate of the electron–hole pairs was faster than their separation rate after the maximum was achieved, resulting in the decreased intensity of the negative TPV response with time, as shown in region III of curve b_2 in Fig. 6(b). In addition, a horizontal area (α-region) appeared in region III of curve b_2 in Fig. 6(b). This phenomenon implied that the lifetime of some photogenerated FCCs was prolonged, because the separation rate of the electron–hole pairs was equal to their recombination rate in this region. The intensity of the negative TPV response of the Mn-doped QDSTF was lower than that of the undoped QDSTF, as compared curve b_2 with b_1 in Fig. 6(b). It seems that the photogenerated FCCs' amount of the former may be less than that of the latter. Consequently, Mn dopant in the QDs helped to change the direction of the photogenerated FCCs transport in the samples, and to prolong the photogenerated FCCs' lifetime in spite of decreasing photogenerated FCCs' amount to a certain extent. For clarity, some relevant parameters extracted by the TPV spectroscopy of the samples are listed in Table 2.

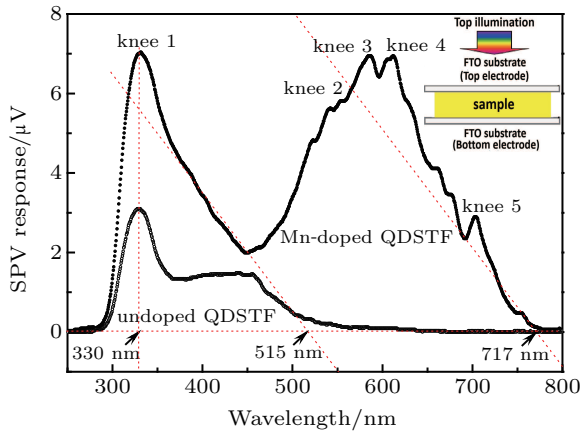

Fig. 7. SPV spectroscopy of the Mn-doped QDSTF and the undoped QDSTF. Inset illustrates the home-build setup for SPV spectrum measurement, in which the experiment irradiation was generated by using a 500 W Xe-arc lamp.

Table 2. Relevant parameters extracted from the UV-VIS absorption spectrum, SPV spectroscopy, and TPV spectroscopy of the as-prepared undoped ZnSe QDs-sensitized nano-TiO_2 thin film and the as-prepared Mn:ZnSe QDs-sensitized nano-TiO_2 thin film.

Sample	Undoped QDSTF	Mn-doped QDSTF				
$E_{g,UV-VIS}$/eV	2.33	1.71				
$E_{g,SPV}$ / eV	2.40	knee 1	knee 2	knee 3	knee 4	knee 5
		3.10	2.29	2.11	2.03	1.73
$I_{max,TPV}$/mV	7.81	5.49				
$I_{max,SPV}$	3.15	7.03				
R_{TPV}/s	$8.36\times10^{-8}-2.70\times10^{-3}$	$7.53\times10^{-8}-6.10\times10^{-3}$				
R_{SPV}/nm	212–581	212–775				

$E_{g,UV-VIS}$ is the optical bandgap of the samples extracted from the UV-VIS absorption spectra; $E_{g,SPV}$ is the photoelectric threshold of the SPV spectroscopy of the samples at the specific wavelength, such as the wavelengths of knees 1–5; $I_{max,TPV}$ represents the absolute maximum of TPV response intensity of the samples illuminated by the laser pulse with a wavelength of 355 nm and an energy of 20 μJ; $I_{max,SPV}$ represents the maximum of SPV response intensity of the samples at 330 nm; R_{TPV} is the region of TPV response of the samples; R_{SPV} is the region of SPV response of the samples.

SPV spectroscopy of La-doped TiO_2 nanoparticles and undoped TiO_2 nanoparticles is displayed in Fig. S4. The photoelectric threshold of main-band gap of both nano-TiO_2 particles above was 3.2 eV, according to the abscissa of the largest external tangent of the band, which was strongly dependent on the band–band transfer transition of the photogenerated carriers in the anatase phase. However, a shoulder peak appeared at the wavelength 422 nm in the SPV spectroscopy of the undoped TiO_2 nanoparticles in Fig. S4. The photoelectric threshold of the shoulder peak was 2.8 eV, which may be related to the band–band transfer transition of the photogenerated carriers in the rutile phase. This result indicated that lanthanum ion doping in nano-TiO_2 may inhibited the formation of rutile phase, which was consistent with the result of Raman spec-

trum in Fig. 3. The SPV spectroscopy of the as-prepared Mn-doped and undoped QDSTFs is shown in Fig. 7. By comparing the SPV spectroscopy of the Mn-doped QDSTF with that of the undoped QDSTF, two outstanding SPV characteristics of the former may be found in Fig. 7. One was that the intensity of the SPV response of the Mn-doped QDSTF at 330 nm was 7.03 μV, which was ∼2.1 times higher than that of the undoped QDSTF. The other was that the region of the SPV response of the Mn-doped QDSTF extended by 191 nm to the long-wavelength region of visible light compared to the undoped QDSTF one, and covered almost the whole visible region. These SPV characteristics of the Mn-doped QDSTF were consistent with the results of the TPV spectroscopy of the samples in Fig. 6. This confirmed that the photovoltaic characteristic of the QDSTF may be greatly improved through doping proper Mn^{2+} ion into the ZnSe QDs sensitizer. Specifically, the photoelectric threshold, $E_{g,SPV}$, of the Mn-doped and undoped QDSTFs was 1.73 eV and 2.40 eV, respectively. These photoelectric thresholds were basically consistent with their respective optical bandgaps obtained by the UV-VIS absorption spectra as listed in Table 2. Knees 1–5 appeared in the SPV spectroscopy of the Mn-doped QDSTF in Fig. 7. Knee 1 located at 330 nm was strongly dependent on the SPV response of the La-doped nano-TiO_2 thin film; knees 2–4 had been identified as the SPV response of the ligand L-Cys, the shell-ZnS, and the core-ZnSe, respectively.[32] As compared with the undoped QDSTF, the SPV responses of knees 2–4 of the Mn-doped QDSTF were red-shift, respectively. The photoelectric threshold of knee 5 should be smaller than that of knees 2–4 because the former was located at the longer wavelength region as compared with the later three knees. Therefore, the lowest excited state level corresponding to knee 5 may be related to the electron level of Mn $2p_{3/2}$ in Fig. 1(f). In other words, the decreased photoelectric threshold of the Mn-doped QDSTF may result from the acceptor level of doped Mn^{2+} ion near and below the bottom of the conduction band of the ZnSe QDs sensitizer as illustrated in Fig. 8. For clarity, some relevant parameters extracted from the SPV spectroscopy of the samples are listed in Table 2.

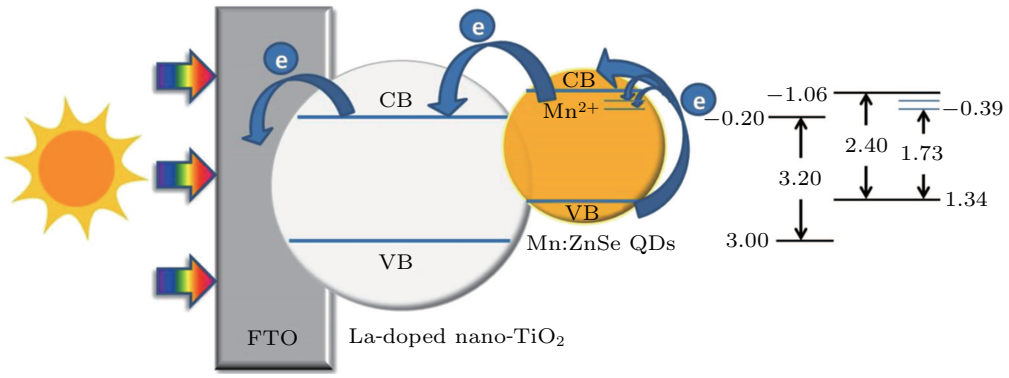

Fig. 8. Schematic diagram of electronic migration and energy levels (eV) in the Mn:ZnSe QDs sensitized La-doped nano-TiO_2 thin film, according to the results extracted from the XPS and the SPV spectroscopy of the as-prepared samples. The band gap of La-doped nano-TiO_2 was extracted from Fig. S4.

4. Conclusions

In summary, the combination of the low temperature aqueous-phase way and the modified CBD method was used to prepare Mn:ZnSe/ZnS/L-Cys core-shell QDs sensitized La-doped nano-TiO_2 thin film. Photoelectron characteristics and microstructure of the Mn-doped QDSTF were probed via XPS and transient and steady state PV technologies, supplemented by FTIR spectrum, UV-VIS absorption spectrum, and laser Raman spectrum. The results confirmed that Mn element was doped into the ZnSe QDs in Mn^{2+} ion form, which partly replaced the vacancy of Zn^{2+} ion and formed MnSe with Se^{2-} ion at the low temperature. The ligand L-Cys not only was a stabilizer of the Mn-doped ZnSe QDs sensitizer, but also played a role of molecular linker between the sensitizer and the substrate. The research revealed that the La-doped nano-TiO_2 thin film provided bigger specific surface and porosity, and was composed of anatase phase with better photoelectric property rather than rutile phase, as compared with the undoped nano-TiO_2 thin film. The results verified that the bottom of the conduction band of the Mn:ZnSe QDs as a sensitizer was just 0.86 eV above that of the substrate thin film. And the acceptor level of the doped Mn^{2+} ion was located at about 0.39 eV below and near the bottom of the conduction band of the QDs. The study confirmed that the Mn-doped QDSTF had a p-type TPV characteristic unlike the undoped QDSTF. The advantages of the Mn-doped QDSTF were strongly dependent on the microstructures mentioned above. Specifically, the intensity of the SPV response of the Mn-doped QDSTF at the specific wavelength was approx. 2.1 times higher than that of the undoped QDSTF. The region of the SPV response of the Mn-doped QDSTF was extended by 191 nm to almost the whole visible region as compared with that of the undoped

QDSTF. The region of the TPV response of the Mn-doped QDSTF also was obviously wider than that of the undoped QDSTF although the extreme of the TPV response of the former was lower than the latter. These outstanding PV characteristics of the Mn-doped QDSTF probably were derived from the prolonged lifetime and extended diffusion length of photogenerated FCCs injected into the La-doped nano-TiO_2 substrate from the Mn:ZnSe QDs sensitizer.

Supplementary material

The adsorption–desorption isotherm and the pore size distribution pattern of the as-prepared TiO_2 nanoparticles are shown in Fig. S1. The results confirmed that the La-doped nano-TiO_2 was a mesoporous material according to the IV-type adsorption–desorption isotherm. The specific surface and porosity of the material were obviously increased by doping lanthanum element into the TiO_2 nanoparticles as listed in Table S1. The result indicated that the nano-TiO_2 thin film deposited on FTO substrate was composed of anatase phase as seen in Fig. S2. A small quantity of MnSe was produced in the doped ZnSe QDs, and the shell-ZnS was formed at between the core-ZnSe and the ligand, as shown in the XRD pattern of the samples in Fig. S3. The result certified that the SPV characteristic of the La-doped TiO_2 nanoparticles was distinctly better than that of the undoped TiO_2 nanoparticles in Fig. S4.

Acknowledgements

We are grateful to Prof. D. J. Wang for his technical assistance, and also to the Metastable Materials Science &Technology of State Key Laboratory, China, for technical and financial support.

References

[1] Kovtun O, Tomlinson I D, Bailey D M, Thal L B, Ross E J, Harris L, Frankland M P, Ferguson R S, Glaser Z, Greer J and Rosenthal S J 2018 *Chem. Phys. Lett.* **706** 741
[2] Delikanli S, Guzelturk B, Hernández-Martínez P L, Erdem T, Kelestemur Y, Olutas M, Akgul M Z and Demir H V 2015 *Adv. Funct. Mater.* **25** 4282
[3] Chistyakov A A, Zvaigzne M A, Nikitenko V R, Tameev A R, Martynov I L and Prezhdo O V 2017 *J. Phys. Chem. Lett.* **8** 4129
[4] Chaguetmi S, Mammeri F, Nowak S and Decorse P 2013 *RSC Adv.* **3** 2572
[5] Chen O, Zhao J, Chauhan V P, Cui J, Wong C, Harris D K, Wei H, Han H S, Fukumura D, Jain R K and Bawendi M G 2013 *Nat. Mater.* **12** 445
[6] Wilson K C, Manikandan E and Ahamed M B 2014 *Mater. Lett.* **120** 295
[7] Milekhin A G, Sveshnikova L L, Repinsky S M, Gutakovsky A K and Friedrich M 2002 *Thin Solid Films* **422** 200
[8] Lohar G M, Shinde S K, Rath M C and Fulari V J 2014 *Mater. Sci. Semicond. Process.* **26** 548
[9] Kennedy J, Murmu P P, Leveneur J, Markwitz A and Futter J 2016 *Appl. Surf. Sci.* **367** 52
[10] Murray C B, Norris D J and Bawendi M G 1993 *J. Am. Chem. Soc.* **115** 8706
[11] Sarma D D, Nag A, Santra P K, Kumar A, Sapra S and Mahadevan P 2010 *J. Phys. Chem. Lett.* **1** 2149
[12] Yu W W, Qu L H, Guo W Z and Peng X G 2003 *Chem. Mater.* **15** 2854
[13] Hughes B K, Beard M C, Nozik A J and Johnson J C 2011 *J. Phys. Chem. Lett.* **2** 1282
[14] Speranskaya E S, Beloglazova N V, Lenain P, Saeger S D, Wang Z, Zhang S, Hens Z, Knopp D, Niessner R, Potapkin D V and Goryacheva I Y 2014 *Biosens. Bioelectron.* **53** 225
[15] Yang Y X, Zheng Y, Cao W R, Titov A, Hyvonen J, Manders J R, Xue J G, Holloway P H and Qian L 2015 *Nat. Photon.* **9** 259
[16] Meinardi F, McDaniel H, Carulli F, Colombo A, Velizhanin K A, Makarov N S, Simonutti R, Klimov V I and Brovelli S 2015 *Nat. Nanotechnol.* **10** 878
[17] Shirasaki Y, Supran G J, Bawendi M G and Bulović V 2013 *Nat. Photonics.* **7** 13
[18] Yan J F and Saunders B R 2014 *RSC Adv.* **4** 43286
[19] Zhu G, Pan L K, Xu T and Sun Z 2011 *ACS Appl. Mater. Inter.* **3** 3146
[20] Song X H, Wang M Q, Shi Y H, Deng J P, Yang Z and Yao X 2012 *Electrochim. Acta* **81** 260
[21] Hossain M A, Jennings J R, Shen C, Pan J H, Koh Z Y, Mathews N and Wang Q 2012 *J. Mater. Chem.* **22** 16235
[22] Lee H J, Wang M K, Chen P, Gamelin D R, Zakeeruddin S M, Gratzel M and Nazeeruddin M K 2009 *Nano. Lett.* **9** 4221
[23] Lee Y L, Huang B M and Chien H T 2008 *Chem. Mater.* **20** 6903
[24] Tian J J, Gao R, Zhang Q F, Li Y W, Lan J, Qu X H and Cao G Z 2012 *J. Phys. Chem. C* **116** 18655
[25] Lin S C, Lee Y L, Chang C H, Shen Y J and Yang Y M 2007 *Appl. Phys. Lett.* **90** 143517
[26] Li G S, Zhang D Q and Yu J C 2009 *Environ. Sci. Technol.* **43** 7079
[27] Huang S Q, Zhang Q X, Huang X M, Guo X Z, Deng M H, Li D M, Luo Y H, Shen Q, Toyoda T and Meng Q B 2010 *Nano Technol.* **21** 375201
[28] Li K Y and Xue Z J 2014 *Mater. Chem. Phys.* **148** 253
[29] Ren L, Li K Y, Cui J Y and Shen T D 2018 *J. Mater Sci: Mater. Electron.* **29** 4478
[30] Li K Y, Shan Q S, Zhu R P, Yin H, Lin Y Y and Wang L Q 2015 *Nanoscale* **7** 7906
[31] Cui J Y, Li K Y, Ren L, Zhao J and Shen T D 2016 *J. Appl. Phys.* **120** 184302
[32] Zhang Y, Xie T F, Jiang T F, Wei X, Pang S, Wang X and Wang D J 2009 *Nanotechnology* **20** 155707
[33] Pernik D R, Turdy K, Radich J G and Kamat P V 2011 *J. Phys. Chem. C.* **115** 13511
[34] Mocatta D, Cohen G, Schattner J, Millo O, Rabani E and Banin U 2011 *Science* **332** 77
[35] Antonelli D M and Ying J Y 1995 *Angew. Chem. Int. Ed. Engl.* **34** 2014
[36] Jing L Q, Sun X J, Xin B F, Wang B Q, Cai W M and Fu H G 2004 *J. Solid. State. Chem.* **177** 3375
[37] Legrand-Buscema C and Bach C M S 2002 *Thin Solid Films* **418** 79
[38] Guijarro N, Shen Q, Gimenez S, Mora-Sero I, Bisquert J, Lana-Villarreal T, Toyoda T and Gomez R 2010 *J. Phys. Chem. C.* **114** 22352
[39] Wei X, Xie T F, Xu D, Zhao Q D, Pang S and Wang D J 2008 *Nanotechnology* **19** 275707
[40] Nakade S, Saito Y, Kubo W, Kanzaki T, Kitamura T, Wada Y and Yanagida S 2004 *J. Phys. Chem. B* **108** 1628
[41] Kronik L and Shapira Y 1999 *Surf. Sci. Rep.* **37** 1
[42] Ren P G, Yan D X, Ji X, Chen T and Li Z M 2011 *Nanotechnology* **22** 055705
[43] Stankovich S, Dikin D A, Piner R D, Kohlhaas K A, Kleinhammes A, Jia Y Y, Wu Y, Nguyen S B T and Ruoff R S 2007 *Carbon* **45** 1558
[44] Park S J, An J H, Piner R D, Jung I, Yang D X, Velamakanni A, Nguyen S B T and Ruoff R S 2008 *Chem. Mater.* **20** 6592
[45] Swart H C, Greeff A P, Holloway P H and Berning G L P 1999 *App. Surf. Sci.* **140** 63
[46] Shenasa M, Sainkar S and Lichtman D 1986 *J. Elecron. Spectrosc.* **40** 329
[47] Mandale A B, Badrinarayanan S, Date S K and Sinha A P B 1984 *J. Elecron. Spectrosc.* **33** 61
[48] Myeongcheol K and Osten H J 1997 *Appl. Phys. Lett.* **70** 2702

[49] Ludeke R, Ley L and Ploog K 1978 *Solid State Commun.* **28** 57
[50] Li K Y, Ren L and Shen T D 2018 *Chin. Phys. B* **27** 067305
[51] Li K Y, Wei S L and Yang W Y 2011 *J. Phys. Chem. Solids* **72** 643
[52] Balaji S, Djaoued Y and Robichaud J 2006 *J. Raman Spectrosc.* **37** 1416
[53] Ma W, Lu Z and Zhang M 1998 *Appl. Phys. A* **66** 621
[54] Ohsaka T 1980 *J. Phys. Soc. Jap.* **48** 1661
[55] Jiang Y, Meng X M, Yiu W C, Liu J, Ding J X, Lee C S and Lee S T 2004 *J. Phys. Chem. B* **108** 2784
[56] Shao Y, Cao C S, Chen S L, He M, Fang J L, Chen J, Li X F and Li D Z 2015 *Appl. Catal. B-Environ.* **179** 344
[57] Xu X Q, Giménez S, Seró I M, Abate A, Bisquert J and Xu G 2010 *Mater. Chem. Phys.* **124** 709
[58] Winter J O, Gomez N, Gatzert S, Schmidt C E and Korgel B A 2005 *Colloids Surf. A: Physicochem. Eng. Aspects.* **254** 147
[59] Mahrov B, Boschloo G, Hagfeldt A, Dloczik L and Dittrich Th 2004 *Appl. Phys. Lett.* **84** 5455
[60] Duzhko V, Koch F and Dittrich Th 2002 *J. Appl. Phys.* **91** 9432
[61] Lifshitz E, Kaplan A, Ehrenfreund E and Meissner D 1998 *J. Phys. Chem. B* **102** 967